Original Article
Multimodal imaging provides insight into targeted therapy response in metastatic prostate cancer to the bone

Benjamin A Hoff[1], Jean-Christophe Brisset[1], Stefanie Galbán[1], Marcian Van Dort[1], David C Smith[2], Zachery R Reichert[2], Jon A Jacobson[1], Gary D Luker[1], Thomas L Chenevert[1], Brian D Ross[1]

Departments of [1]Radiology, [2]Internal Medicine, University of Michigan, Ann Arbor, Michigan, United States of America

Abstract: Metastatic prostate cancer to bone remains incurable, driving efforts to develop individualized, targeted therapies to improve clinical outcomes while limiting adverse side-effects. Due to the complexity in cellular signaling pathways and the interaction between cancer and its microenvironment, multiparametric imaging approaches for treatment response may improve understanding of the biological effects of therapy. An orthotopic model of castration resistant prostate cancer (CRPC) bone metastasis was treated with the tyrosine kinase inhibitor Cabozantinib (CABO). Response was assessed using CT to monitor bone volumes, ^{99m}Tc-MDP SPECT for bone metabolism, and anatomical and diffusion MRI for tumor volume and cell death. A concurrent clinical trial of CABO for CRPC patients also evaluated multimodality imaging in correlation with standard response criteria. Response in the preclinical study found significant slowing in tumor growth rate (P<0.01), rise in tumor apparent diffusion coefficient (ADC, P<0.001), and drop in ^{99m}Tc-MDP adsorption (P<0.05). Loss of bone volume did not slow with treatment, attributed to the highly aggressive and osteolytic nature of the PC3 cell line. Clinical trial analysis found only a single subject who progressed after 12 weeks of therapy. Imaging at 6 weeks corroborated the 12-week radiological assessment with positive response visible as increased ADC and decreased vascular metrics. Conversely, the subject who progressed at 12 weeks had no change in ADC, and substantial drops in vascular metrics. These results showcase a multifaceted translational imaging approach for detecting targeted treatment response with effective blockade of tumor vascularization, tumor cell kill, and reduced proliferation.

Keywords: Prostate cancer, bone metastasis, cabozantinib, imaging, treatment response, parametric response map, imaging biomarker

Introduction

Prostate cancer has one of the highest incidence rates among all cancers, accounting in the US for approximately 19% of new cases and 8% of cancer related mortality in 2017 [1]. Bone metastases are the main cause of morbidity and mortality in prostate cancer, affecting 65-75% of men with advanced disease [2]. Metastatic prostate cancer disrupts normal bone architecture through a cellular signaling "vicious cycle", resulting in progressive local loss of structural integrity and resistance to conventional therapies [3]. The standard-of-care for treatment of metastatic prostate cancer remains chemical or surgical reduction of systemic androgens. However, cancer cells almost invariably become independent of androgens (castration-resistant prostate cancer, CRPC), leading to lethal disease.

Recent advances in molecular mechanisms of cancer have ignited interest in development of targeted therapies for a more individualized approach to cancer therapy. Targeted therapies are designed to affect specific pathways involved in cancer promotion and proliferation while minimizing adverse effects on normal bodily tissues and structures. Such therapies may target cancer cells and/or components of a tumor microenvironment, such as bone in prostate cancer. Bone-targeted agents, such as bisphosphonates and RANK (receptor activator of nuclear factor kappa B) ligand inhibitors, are

already widely used in clinical practice to prevent bone degradation and reduce micro-environmental stimulation of cancer metastases. Cabozantinib (CABO) is a small-molecule tyrosine kinase inhibitor that inhibits c-Met and VEGFR2. CABO simultaneously inhibits metastasis, angiogenesis, and proliferation in animal tumor models [4] and has recently concluded phase III clinical trials for men with CRPC bone metastases with negative efficacy [5].

Current clinical criteria for determination of treatment response and progression of bone metastases is lacking. Osteolytic bone metastases with soft tissue masses greater than 1 cm are considered measurable disease, but sclerotic bone lesions remain unmeasurable [6, 7]. Clinical management of bone disease has historically relied heavily upon bone scintigraphy using ^{99m}Tc-methyl diphosphonate (^{99m}Tc-MDP) to highlight bone remodeling, but such readouts may be misleading due to their indirect measurement of tumor involvement [8-10]. Because of the known interaction between metastatic prostate cancer cells and their micro-environment, a multifaceted imaging approach to monitor metastatic tumor response to treatments may be more clinically accurate while providing insights into underlying biological signaling pathways involved in response and progression of this disease [11].

In this study, CABO treatment response in an orthotopic mouse model of prostate cancer bone metastases was evaluated using multiple imaging modalities, including MRI to monitor soft tissue volumes and cell death via the apparent diffusion coefficient (ADC), X-ray computed tomography to monitor bone structural changes, and MDP-SPECT to monitor sclerotic activity. Therapeutic effects were evident as slowed tumor growth, a transient increase in tumor ADC, and a reduction in ^{99m}Tc-MDP adsorption compared to control animals. In addition to our preclinical disease studies, imaging was incorporated into a concurrent clinical trial to assess early therapeutic efficacy of CABO. In addition to bone scintigraphy and x-ray CT guided biopsy, diffusion MRI was also acquired at baseline and following 6 weeks of therapy. Parametric response mapping of tumor ADC values at 6 weeks identified the single subject with progressive disease defined by standard criteria at week 12. The results of this study demonstrate feasibility and significant prognostic potential for including multi-modality imaging readouts for evaluation of targeted cancer therapies, both during preclinical drug development as well as in clinical trials.

Materials and methods

Cell culture

Androgen independent (hormone refractory) human prostate cancer [12] cells (PC3) were purchased from American Type Culture Collection (ATCC, Manassas VA). The cells were grown as monolayers in 10 cm^2 sterile plastic flasks in Roswell Park Memorial Institute medium (RPMI 1640) with 10% fetal bovine serum, 100 IU/mL penicillin, 100 mg/mL streptomycin, 2 mmol/L L-glutamine in a humidified incubator at 37°C in 5% CO_2. Prior to implantation, cells were harvested by trypsinization, counted, and suspended in serum-free medium for injection.

Animal model

All studies involving the use of mouse protocols were approved by the University of Michigan Institutional Animal Care & Use Committee (IACUC). Male severe combined immunodeficient (SCID) mice were included in the study at 4-6 weeks of age and were maintained according to the NIH standards established in the "Guidelines for the Care and Use of Laboratory Animals" in specific pathogen-free housing. For implantation of prostate cancer cells, mice were anesthetized by intraperitoneal injection of a mixture of ketamine (100 mg/kg body wt., Ketaset, Aveco Co, Fort Dodge, IA) and xylazine (10 mg/kg, AnaSed, Lloyd Laboratories, Shenandoah, IA). Right tibias were depilated and cleaned with an alcohol wipe. A Hamilton syringe with a 28-gauge needle was inserted in the middle of the patella ligament through the tibial crest epiphysis and growth plate. Carprofen (5 mg/kg, Rimadyl, Pfizer, New York, NY) was injected subcutaneously at the end of the procedure as an analgesic. PC3 cells (5×10^5) suspended in 10 µl of serum-free media were injected into the trabecular bone of the tibial metaphysis. Sham surgeries were performed on the left leg using an identical procedure but injecting media only.

Targeted therapy

Animals were separated into treatment groups once tumor volumes reached approximately 20

mm^3, as determined by MRI. Treatment with Cabozantinib (CABO, Exelixis, Inc.) was administered daily for 21 days via oral gavage at a dose of 30 mg/kg in a 10% DMSO solution in PBS (n = 8) [13]. Control animals were given vehicle alone (n = 12). Animal body weights were monitored throughout the study as an indicator of dose toxicity and were not found to drop below 15% reduction within the course of the study. Experimental endpoints were determined when tumor volumes exceeded 200 mm^3.

Magnetic resonance imaging (MRI)

Anatomical and diffusion MRIs were acquired on the day before the first treatment and twice weekly thereafter until the end of the study. Imaging was performed using a 9.4 T, 12 cm horizontal bore Agilent (Santa Clara, CA) *Direct Drive* system with a quadrature 20 mm volume coil (m2m Imaging, Cleveland, OH) with the leg securely fastened within the coil to reduce motion. During MRI examinations, animals were anesthetized with 1.5% isoflurane/air, and body temperature was maintained by blowing warm air through the bore of the magnet (Air-Therm, World Precision Instruments, Sarasota, FL). Diffusion weighted images (DW-MRI) were acquired using a spin-echo sequence, with a navigator echo and gradient waveforms sensitive to isotropic diffusion [14] with the following parameters: repetition time (TR)/echo time (TE) = 4000/37 msec, field of view (FOV) = 20×20 mm^2, matrix size = 128×64, slice thickness = 0.5 mm, number of slices = 40, bandwidth = 50 kHz, gradient pulse width = 10.5 msec, gradient pulse separation = 25 msec, and b-values (x-gradient, y-gradient, and z-gradient amplitudes) of 120 (7.9, 7.1, and 5.2 G/cm) and 1200 (24.5, 22.5, and 17.8 G/cm) s/mm^2.

Tumor volumes of interest (VOI) were delineated manually on the high-b diffusion image, while also referencing the anatomical T2-weighted image. The apparent diffusion coefficient (ADC) maps were generated using the standard two-point subsampling of the signal decay curve using a mono-exponential model.

Micro X-Ray computed tomography (μCT)

μCT imaging was performed weekly until the end of the study. Images were acquired using a

Siemens Inveon system (Knoxville, TN) with the following acquisition parameters: 80 kVp, 500 μA, 300 ms exposure, 501 projections over 360 degrees and 56 μm reconstructed voxel size. During image acquisition animals were sedated via inhalation of 2% isofluorane in air and positioned supine with both legs secured with tape in an extended position.

All quantitative CT images were calibrated to Hounsfield units (HU) using a water phantom placed in the FOV alongside the animal. Tibia VOIs were delineated using an in-house semi-automated region-growing algorithm including regions over a threshold of 500 HU and encompassing the bone between the tibial plateau and the tibia/fibula junction.

^{99m}Tc-MDP SPECT

A subgroup of animals was subject to weekly ^{99m}Tc-MDP bone scans in addition to the other imaging acquisitions (5 controls and 4 CABO-treated). ^{99m}Tc-MDP was diluted with PBS and injected via lateral tail vein at a dose of approximately 2 mCi in 100-150 μL per mouse 3 hours before image acquisition to allow time for bladder clearance. Imaging was performed using an explore speCZT CT 120 system (Tri-Foil Imaging, Chatsworth, CA) equipped with a 7-pinhole collimator and the following acquisition parameters: 40 steps, 30 sec/step, 1° step size, and reconstructed energy window of 125-150 kV. Images were spatially aligned with the corresponding CT image using an automated algorithm (MIAMI Fuse; University of Michigan, Ann Arbor, MI) using a rigid body transformation and mutual information as the cost function [15]. Images were quantified using the VOI drawn on the CT image as the change in ratio of mean activities (R_{Tc} = tumor-bearing tibia activity/sham tibia activity) for each animal.

Clinical trial

Subjects were accrued as part of an approved clinical trial performed at the University of Michigan (NCT01428219) for investigation of CABO as therapy for prostate metastases in the bone. All patients voluntarily underwent Informed Consent prior to inclusion into the clinical trial. Briefly, the clinical trial enrolled subjects with castrate resistant prostate cancer treated orally with CABO monotherapy (60
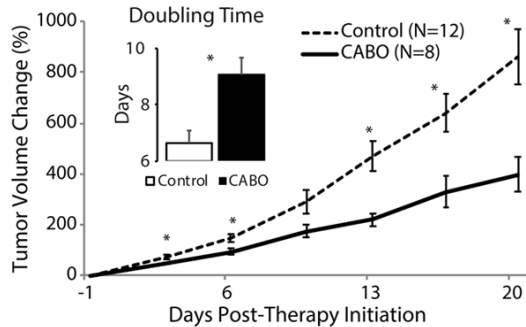
Figure 1. Mean group tumor volumes monitored over time using anatomical MRI show a significant slowing of tumor growth with CABO therapy. A significant difference between group mean volumes (P<0.05) was detected at 3 days post-treatment initiation. The embedded bar plot shows a significant difference (P<0.01) between mean group tumor doubling times for control (white bar, 7.0±0.5 days) and CABO (black bar, 9.4±0.6 days). Errors displayed are SEM, and significant differences between groups (P<0.05) is indicated by *.

mg daily). Bone scans (^{99m}Tc-MDP scinitigraphy) and chest/abdominal and pelvic CTs were acquired pre-treatment and at 6 and 12 weeks post-initiation. Additionally, pre-treatment and at 6 weeks, a selected bone metastatic lesion was biopsied for histological assessment of treatment-related tumor changes, and quantitative magnetic resonance imaging (MRI) was performed using a Philips 3T scanner. The MRI protocol included: diffusion-weighted (DW-) MRI using a spin-echo prepared echo planar imaging acquisition and b-values of 0 and 1000 s/mm^2; dual-angle T1-mapping acquisition; dynamic contrast-enhanced (DCE-) MRI; T1-weighted SPIR acquisitions pre- and post-contrast administration. A second pre-treatment DW-MRI acquisition was also acquired as a test-retest process in order to estimate the confidence interval of ADC value reproducibility to determine the threshold for statistically significant change in diffusion values. DCE-MRI was quantified using the Tofts-Kermode two compartment model, resulting in metrics of vascular efflux rate (K^{Trans}), extracellular volume fraction (v$_e$), blood plasma volume fraction (v$_p$), and the normalized area under the curve (NAUC). Subjects were excluded if initial tumor volume was under 5 cm^3 to avoid partial-volume effects.

Parametric response maps (PRM)

Parametric Response Maps [16] were used to detect changes in quantitative imaging ADC metrics on a voxel scale [17-19]. This process involved image co-registration using an automated iterative image transformation algorithm wherein each lesion was co-registered individually using a thin-plate spline warping interpolant. After registration, each image voxel is then ascribed with two quantitative indices, one pre-treatment and the other post-treatment (or a second scan in the test-retest exam). Image voxels were statistically classified by their change over time using a threshold determined by the 95% confidence interval found in images obtained the same day (test-retest data) into one of the following categories: increased (PRM$_{ADC+}$, red), decreased (PRM$_{ADC-}$, blue), or unchanged (PRM$_{ADC0}$, green). PRM analysis was applied to ADC values as a measure of change in tumor cellularity [20-23].

Statistics

Group comparisons were performed using a two-tailed Student's t-test. Significant difference between groups was assessed by P<0.05. All data was presented as the mean ± the standard error of the mean (SEM).

Results

Preclinical

Intratibial tumors reached their predetermined starting volume approximately three weeks post-implantation as measured by anatomical MRI (19±0.7 mm^3). Change in tumor volumes (**Figure 1**) revealed a reduced volumetric growth rate in the CABO-treated mice (9.4±0.6 days doubling time, P<0.01) compared to controls (7.0±0.5 days doubling time). The percent change in tumor volume showed a significant difference between groups as early as three days post-treatment and remained below control values throughout the course of treatment. At the conclusion of CABO treatment (day 21 post-initiation) tumor volumes appeared to accelerate and lost significance in comparison to the control group indicating a possible recovery to pre-therapy growth rate.

Diffusion MRI (**Figure 2**) was used to evaluate for cell death during treatment with CABO, revealing a heterogeneous response to CABO treatment (ADC map overlays, **Figure 2A**). Imaging data with excessive motion or other artifact were excluded from analysis. There is a clearly visible region of high ADC in the CABO-
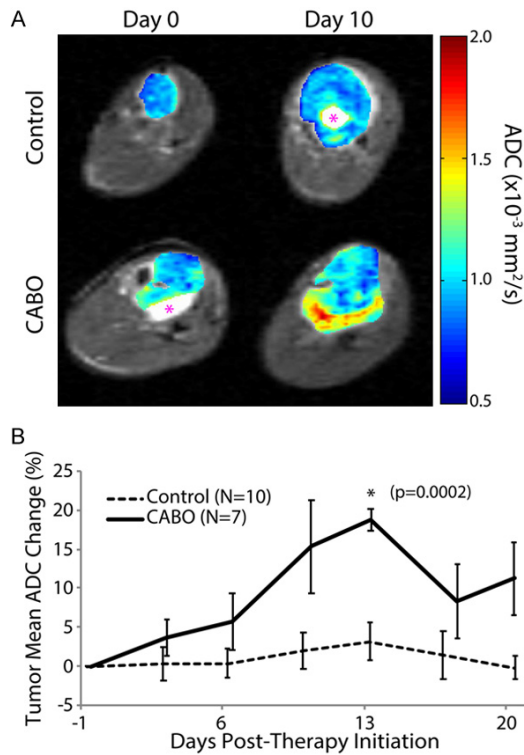
Figure 2. Diffusion MRI analysis revealed an increase in mean tumor ADC for the CABO-treated mice over controls as shown by (A) representative ADC maps overlaid on anatomical images for pre- and 10 days post-treatment initiation. Regions of edema (indicated by asterisk) were excluded from analysis. (B) The change in ADC became significant (P<0.001) on day 13 post-treatment (+18.7±1.5% in the CABO group, and +3.1±2.4% for controls). Data are presented as mean ± SEM, and significant differences between groups (P<0.05) are indicated with *.

Figure 3. In vivo µCT imaging revealed progressive erosion of bone local to the growing tumor for both control and CABO-treated groups. A. Representative isosurfaces of the tumor-bearing tibia for a control and treated mouse are displayed showing substantial bone degradation in both groups over the time period of treatment (3 weeks). B. A plot of the change in bone volume over time shows no significant difference between groups at any time point during the study. Data are presented as means +/-SEM.

treated animal on day 10, which is the driving force behind the increasing mean tumor ADC measurement. Areas of very high ADC (**Figure 2A** asterisk) were excluded from analysis by contouring the tumor using the high b-value image in order to focus on solid tumor response. **Figure 2B** shows a slow increase in mean tumor ADC for the CABO-treated group, peaking around 13 days post-treatment (+18.7±1.5%; P<0.001) over control animals (+3.1±2.4%) and remaining elevated throughout the study.

Monitoring bone volumes over time was accomplished using *in vivo* µCT imaging (**Figure 3**). These studies revealed a predominantly osteolytic tumor phenotype with progressive bone erosion in both groups when visualized as bone isosurfaces (**Figure 3A**). In both representative tibiae, the tumor has already eroded through

the bone around the implant site on the pretreatment time point and continued throughout the study. **Figure 3B** shows no significant reduction in bone loss for the CABO-treated group compared to controls at any time point, indicating that although tumor growth rate has been inhibited the osteolytic process of the bone-tumor interaction remained unimpeded.

99mTc-MDP SPECT is an important imaging modality for monitoring CABO clinical activity, thus corollary studies were also undertaken in the mouse groups. Maximum intensity projection (MIP) overlays (**Figure 4A**) show elevated uptake of 99mTc-MDP in bone in the region of the tumor where bone tissue was still present. The highest uptake was seen in the growth plate, which was excluded from quantitative analysis to be more sensitive to tumor-related
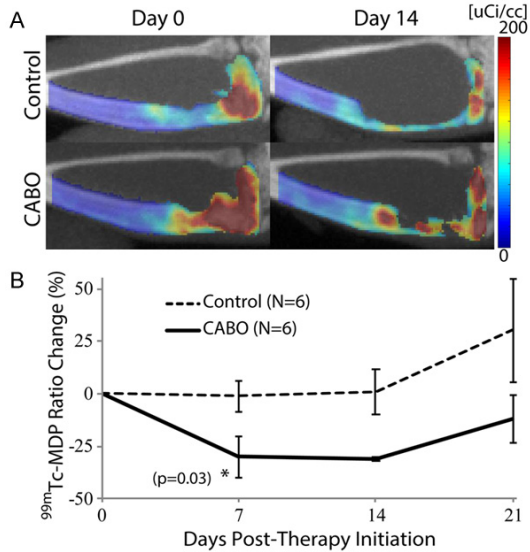
Figure 4. SPECT imaging revealed a drop in mean signal ratio after CABO treatment. A. Representative SPECT MIP maps are overlaid on CT MIP for a control and a treated animal pre- and 2 weeks post-treatment initiation show elevated signal in regions of tumor-bone interface, where bone remodeling is accelerated by the tumor. B. A plot of the change in SPECT signal shows a significant drop after one week of treatment ($P<0.05$) in the CABO -treated group ($-30\pm9.7\%$) compared to controls ($-1.2\pm7.4\%$). Data are presented as mean $\pm$ SEM, and significant difference between groups ($P<0.05$) is indicated by *.

Table 1. Comparison of multiparametric change between progression-free groups at 12 weeks

Progression-Free (12 wks)		*Yes*	*No*
N		12	1
Volume Change (%)		-8.3 (9.5)	-10.3
ADC	% Change	35.1 (12.6)	3.9
	PRM_{ADC+} (%)	44.5 (7.4)	9.5
	PRM_{ADC-} (%)	10.9 (3)	6.2
DCE-MRI	K^{Trans} (%)	-73.5 (13.1)	313.9
	v_e (%)	-59.8 (11.5)	117.2
	NAUC (%)	-75.5 (12.8)	185

Values represent: mean with SEM in parentheses.

activity. The change in mean ^{99m}Tc-MDP activity ratio, R_{Tc}, was monitored weekly (**Figure 4B**) and revealed a decrease for the CABO-treated group ($-30.1\pm9.7\%$) compared to controls ($-1.2\pm7.4\%$), which was significant on day 7 post-treatment ($P<0.05$). SPECT activity ratios at later time points, however, were obscured by the progressive loss of bone resulting in a lower surface area for ^{99m}Tc-MDP binding.

Clinical

Of the 29 subjects enrolled in the study, many were excluded from this analysis due to the following reasons: initial tumor volume was too small (n = 5), initial screen of patient entrance criteria was inadequate (n = 7), or follow-up imaging was not available (n = 4). Soft tissue masses of less than 5 cm^3 were excluded from analysis due to the confounding effect of partial-volume signal on diffusion measurements. For the remaining subjects (n = 13), all were determined to be progression-free at 6 weeks (PF6), and 12 subjects were clinically found to be progression-free at 12 weeks (PF12). The single subject that was determined to have progressed at 12 weeks was due to a new liver metastasis. During the course of the study, 5 subjects dropped out due to adverse side effects from therapy and 7 subjects showed clinical progression concurrent with therapy. For those who progressed during therapy, time to progression ranged from 12 to 96 weeks with a median progression free survival of 28 ± 5 weeks.

To set the threshold for detection of significant change in ADC values, patients underwent test-retest MRI scans separated by less than one hour. Voxel-wise comparison between registered pre-treatment ADC measurements resulted in a population-mean 95% confidence interval of 0.26×10^{-3} mm^2/s. This threshold was then used as a cutoff to determine voxel-wise significant change in ADC values between pre- and 6 weeks post-CABO treatment in the PRM analysis. Although all subjects were found to be progression-free at 6 weeks using clinical radiological response criteria, PRM_{ADC+} was found to be lowest (9.5%) in the single subject that progressed before week 12, compared to $44.5\pm7.4\%$ in the subjects that were progression-free at 12 weeks (**Table 1**). A substantial difference in soft tissue volume change for this same unresponsive subject was not found. Intratumoral heterogeneity in ADC response was evident by PRM overlays, and representative bone scans demonstrated lower sclerotic activity in all subjects (**Figure 5**).

DCE-MRI was used to assess changes in vascular characteristic due to therapy in 8 subjects, with four subjects not able to complete the dynamic study due to patient non-compliance. Vascular volume fractions (v_p) at baseline
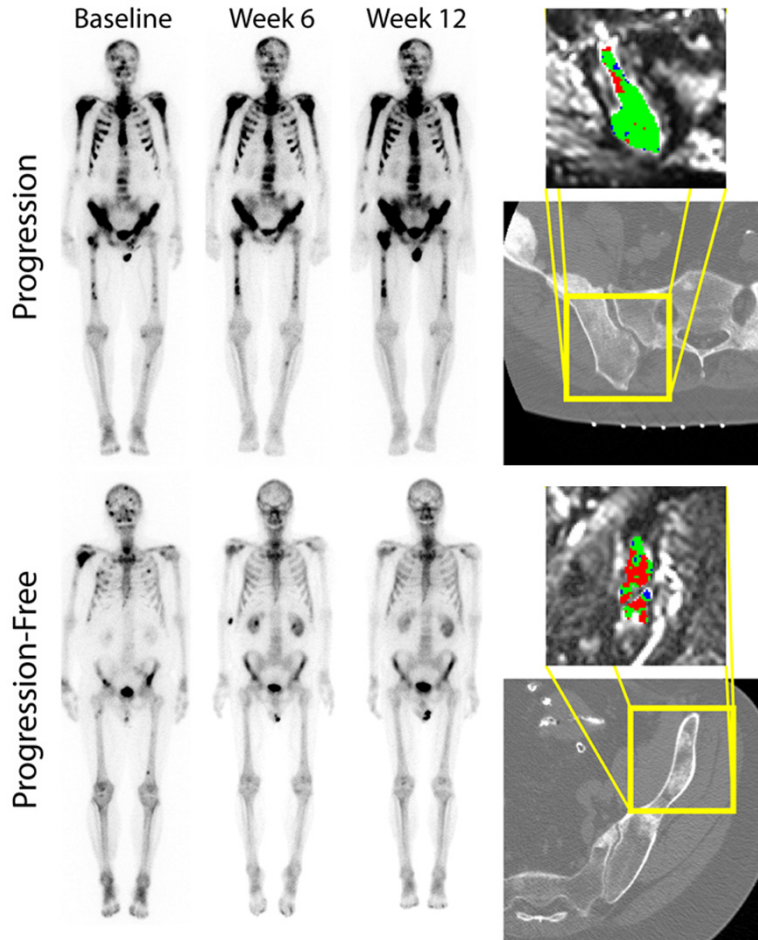
Figure 5. Imaging results of the clinical trial revealed only a single subject that was not progression-free at 12 weeks (non-PF12). Bone scintigraphy (left) shows progressively increasing uptake in the non-PF12 subject (top), while a representative PF12 subject (bottom) had progressively decreased uptake between studies, with many small lesions throughout the skeletal system disappearing by 6 weeks post-therapy. Parametric Response Maps (PRM, right) of tumor ADC between baseline and 6 weeks shows a clear increase (red, PRM$_{ADC+}$) in the PF12 subject, indicating tumor cell kill, but very little change in the non-PF12 subject.

hological evaluation of cancer treatment response, i.e. change in tumor volume or growth rate, is not sufficient for these cases (RECIST 1.1, [6, 24]). The apparent diffusion coefficient (ADC) derived from diffusion weighted MRI has shown great promise to detect tumor cell death in response to therapy. However, imaging strategies including more direct treatment-specific effects could provide additional insight for clinical management. Recent efforts have highlighted a critical interaction between metastatic cancer and its local micro-environment, providing a protective niche and enhancing proliferation [25]. Multimodal imaging has shown promise in evaluating treatment response in mouse models of bone metastasis, including readouts not only of tumor morphology but also tumor cellular signaling and microenvironment [11, 26]. Additionally, cancer therapeutics are progressing toward individualized treatment strategies to mitigate side-effects while maximizing therapeutic efficacy. Therefore, tailoring imaging strategies to individual cases based on genomics and treatment strategies are anticipated to provide a more comprehensive readout for determination of treatment efficacy.

While CRPC currently remains incurable, the progressively improving understanding of oncological driver mutations and signaling is spurring development of targeted therapies that have shown promise for this disease. One such agent, the small molecule kinase inhibitor Cabozantinib (CABO), is a potent inhibitor of MET and VEGFR2 [4], which are highly expressed in bone-metastatic prostate cancers, as well as other receptor tyrosine kinases implicated in cancer pathology [27, 28]. Activation

were insubstantial in all but one case, so relative change in v$_p$ was not evaluated in this study. PF12 subjects had consistent decreases in K^{Trans}, v$_e$, and NAUC (**Table 1**), indicating a renormalization of tumor vasculature with lower permeability. The non-PF12 subject had substantial increases in all three metrics, indicating a progression in vascular recruitment and permeability.

Discussion

Treatment and response evaluation of bone metastases is a significant challenge and focus of continuing research efforts. Morp-

of MET and VEGFR2 in cancer promote angiogenesis, while MET is implicated in cellular proliferation, dissociation leading to metastasis, and activation of key oncogenic pathways such as RAS, PI3K, STAT3, and β-catenin. Studies suggest the MET pathway correlates with CRPC [29]. Expression of c-MET mRNA was detected in the PC-3 cell line but not the more sclerotic LNCaP cell line [27]. In the present study, inhibition of these pathways in the mouse orthotopic model using CABO reduced tumor growth rate compared to controls (**Figure 1**) and caused a transient increase in tumor ADC values (**Figure 2**) which indicates reduced proliferation with greater cell death. Mean tumor ADC values were also shown to increase between baseline and 6 weeks for the majority of subjects in the clinical trial. PRM of tumor ADC values was performed in these clinical subjects to potentially provide a more comprehensive and spatially-resolved readout of intratumoral changes, resulting in PRM_{ADC+} values at 6 weeks that agreed with radiological assessment at 12 weeks (**Figure 5**).

Vasculature is critical to maintain a high rate of cellular proliferation observed in cancer due to its need for nutrients. Neovascularization in cancer is often driven by hypoxia as well as overexpression of angiogenic factors, such as vascular endothelial growth factor (VEGF), and down-regulation of angiogenic inhibitors by cancer cells [30]. Previous studies have shown the utility of dynamic contrast MRI for monitoring cancer response to vascular-targeted therapies [31-34]. Preclinical and clinical studies have reported transient tumor vascular response to VEGF-targeted therapy followed by resumption of tumor growth and progression with increased invasiveness, indicating development of therapy resistance [35, 36]. MET has been shown to play an important role in the development of resistance to VEGF inhibition [37-39], so inhibition of both VEGF and MET pathways by CABO treatment should improve disruption of cancer angiogenesis [4]. The presented clinical study found a single subject who did not have a drastic reduction in K^{Trans} or NAUC at week 6. This subject was also determined to radiologically have clinical disease progression at week 12 which appears to correlate with the unresponsiveness of this subject. While limited patient accrual limits further statistical evaluation, this anecdotal evidence supports the role of further investigations into multi-modal imaging to provide additional treatment responsiveness assessment in this patient population.

The interaction between metastatic bone cancer and its local host tissue bone microenvironment has been termed the "vicious cycle" of bone metastasis [3, 40-42]. This hypothesis proposes that the invading cancer cells induce osteoclastic activity through secretion and promotion of osteoclast-activating factors and osteoblast inhibiting factors. Metastatic bone lesions commonly release cytokines that upregulate RANK ligand (receptor activated nuclear factor-κB) production of osteoblast (OB) precursors, resulting in increased osteoclast (OCL) activity. Resorption of bone tissue releases and activates growth factors from the bone matrix, such as TGF-β, that further stimulates tumor growth and continuing the cyclical process. Normal bone remodeling is dependent on tight communication between OCL expression of ephrins and OB-expressed Eph receptors [43]. Because bone metastases cause an imbalance in OCL and OB activity, local bone homeostasis is lost, which may result in bone resorption or deposition of abnormal bone. Due to this interaction, monitoring of microenvironmental changes in addition to the soft-tissue components may provide additional biological insights and underpin improvements in the sensitivity of imaging to be used in the context of precision medicine. In this regard, X-ray CT was performed to monitor changes in bone volume and guide stereotactic biopsy, while bone scintigraphy (^{99m}Tc-MDP) was used to monitor overall osteosclerotic activity. Response in bone scan activity was seen both in the preclinical study and the clinical subjects as a reduction in ^{99m}Tc-MDP adsorption, which indicated a CABO-associated re-normalization of bone metabolism local to the tumor had occurred.

The PC3 cancer cell line used in this study is well established for use in orthotopic mouse models of bone-metastatic disease with high metastatic potential [12, 16, 44]. The cell line originated from a grade IV prostatic adenocarcinoma from a 62-year old male Caucasian, is androgen independent, and does not express elevated prostate-specific antigen [12]. This cell line is highly aggressive and has been shown to drastically increase bone resorption local to the tumor [16]. Although CABO therapy

slowed tumor growth in this study, it did not halt or reverse progression and produced no significant reduction in the observed progressive rate of bone resorption (**Figure 3**). Nonetheless, a significant drop in ^{99m}Tc-MDP adsorption was found 1-2 weeks post-therapy, indicating a therapeutic effect on cancer-bone interaction was achieved. ^{99m}Tc-MDP bone scintigraphy results are known to be difficult to interpret in bone lesions with high osteolytic activity and rapid bone damage [45], but our results show promise for this targeted agent. An independent study by Graham et al. [26] also using a multimodality approach to assess CABO in mice also reported both anti-tumor activity by slowing tumor growth with an increased tumor ADC along with an osseous response of decreased ^{99m}Tc-MDP uptake and normalization of bone structure via CT analysis. Graham et al. used VCaP cells, an androgen independent prostate cancer originating from a metastatic lesion to a lumbar vertebra of a 59-year-old Caucasian. These cells are less aggressive and exhibit lower metastatic potential. The VCaP tumor model is known to mimic the osteo-metabolic activity of clinical disease with local sclerotic remodeling of bone, contrasting with the highly osteolytic nature of the PC3 tumor model. The difference in bone response shown between this study and that of Graham et al. highlights the variability of response metrics between seemingly similar disease, necessitating a multifaceted imaging strategy for robust assessment of therapeutic response.

In conclusion, our multi-modality imaging approach was able to detect and quantify both tumor and bone responses to CABO therapy. Imaging of vascular response to CABO (DCE-MRI) was vital to show a direct therapeutic response, while diffusion MRI captured cancer cell death and bone scintigraphy/SPECT detected a positive bone-metabolic response. Clinical cancer patient management is continually progressing toward personalized medicine based on genetically-informed, targeted treatments. Targeted therapies may not directly induce tumor cell death. Moreover, treatments may also have a significant impact on stromal or immunological tissue types that can impact overall tumor progression. Multiparametric imaging response metrics may improve our understanding of the biological effects of therapy and lead to improved treatment response rates, patient management and clinical outcome.

Disclosure of conflict of interest

None.

Address correspondence to: Dr. Brian D Ross, Department of Radiology, Center for Molecular Imaging, Biomedical Sciences Research Building, University of Michigan, 109 Zina Pitcher Place, Ann Arbor, MI 48109, Michigan, United States of America. Tel: 734-763-2099; E-mail: bdross@umich.edu

References

[1] Siegel RL, Miller KD and Jemal A. Cancer statistics, 2017. CA Cancer J Clin 2017; 67: 7-30.

[2] Coleman RE. Metastatic bone disease: clinical features, pathophysiology and treatment strategies. Cancer Treat Rev 2001; 27: 165-176.

[3] Mundy GR. Metastasis to bone: causes, consequences and therapeutic opportunities. Nat Rev Cancer 2002; 2: 584-593.

[4] Yakes FM, Chen J, Tan J, Yamaguchi K, Shi Y, Yu P, Qian F, Chu F, Bentzien F, Cancilla B, Orf J, You A, Laird AD, Engst S, Lee L, Lesch J, Chou YC and Joly AH. Cabozantinib (XL184), a novel MET and VEGFR2 inhibitor, simultaneously suppresses metastasis, angiogenesis, and tumor growth. Mol Cancer Ther 2011; 10: 2298-2308.

[5] Smith M, De Bono J, Sternberg C, Le Moulec S, Oudard S, De Giorgi U, Krainer M, Bergman A, Hoelzer W, De Wit R, Bogemann M, Saad F, Cruciani G, Thiery-Vuillemin A, Feyerabend S, Miller K, Houede N, Hussain S, Lam E, Polikoff J, Stenzl A, Mainwaring P, Ramies D, Hessel C, Weitzman A and Fizazi K. Phase III study of cabozantinib in previously treated metastatic castration-resistant prostate cancer: COMET-1. J Clin Oncol 2016; 34: 3005-3013.

[6] Costelloe CM, Chuang HH, Madewell JE and Ueno NT. Cancer response criteria and bone metastases: RECIST 1.1, MDA and PERCIST. J Cancer 2010; 1: 80-92.

[7] Scher HI, Morris MJ, Stadler WM, Higano C, Basch E, Fizazi K, Antonarakis ES, Beer TM, Carducci MA, Chi KN, Corn PG, de Bono JS, Dreicer R, George DJ, Heath EI, Hussain M, Kelly WK, Liu G, Logothetis C, Nanus D, Stein MN, Rathkopf DE, Slovin SF, Ryan CJ, Sartor O, Small EJ, Smith MR, Sternberg CN, Taplin ME,

Wilding G, Nelson PS, Schwartz LH, Halabi S, Kantoff PW, Armstrong AJ; Prostate Cancer Clinical Trials Working Group 3. Trial design and objectives for castration-resistant prostate cancer: updated recommendations from the prostate cancer clinical trials working group 3. J Clin Oncol 2016; 34: 1402-1418.

[8] Abdel-Dayem HM. The role of nuclear medicine in primary bone and soft tissue tumors. Semin Nucl Med 1997; 27: 355-363.

[9] Hamaoka T, Madewell JE, Podoloff DA, Hortobagyi GN and Ueno NT. Bone imaging in metastatic breast cancer. J Clin Oncol 2004; 22: 2942-2953.

[10] Miller TT. Bone tumors and tumorlike conditions: analysis with conventional radiography. Radiology 2008; 246: 662-674.

[11] Hoff BA, Chughtai K, Jeon YH, Kozloff K, Galban S, Rehemtulla A, Ross BD and Galban CJ. Multimodality imaging of tumor and bone response in a mouse model of bony metastasis. Transl Oncol 2012; 5: 415-421.

[12] Kaighn ME, Narayan KS, Ohnuki Y, Lechner JF and Jones LW. Establishment and characterization of a human prostatic carcinoma cell line (PC-3). Invest Urol 1979; 17: 16-23.

[13] Wang X, Huang Y, Christie A, Bowden M, Lee GS, Kantoff PW and Sweeney CJ. Cabozantinib inhibits abiraterone's upregulation of IGFIR phosphorylation and enhances its anti-prostate cancer activity. Clin Cancer Res 2015; 21: 5578-5587.

[14] Chenevert TL, McKeever PE and Ross BD. Monitoring early response of experimental brain tumors to therapy using diffusion magnetic resonance imaging. Clin Cancer Res 1997; 3: 1457-1466.

[15] Meyer CR, Boes JL, Kim B, Bland PH, Zasadny KR, Kison PV, Koral K, Frey KA and Wahl RL. Demonstration of accuracy and clinical versatility of mutual information for automatic multimodality image fusion using affine and thin-plate spline warped geometric deformations. Med Image Anal 1997; 1: 195-206.

[16] Brisset JC, Hoff BA, Chenevert TL, Jacobson JA, Boes JL, Galban S, Rehemtulla A, Johnson TD, Pienta KJ, Galban CJ, Meyer CR, Schakel T, Nicolay K, Alva AS, Hussain M and Ross BD. Integrated multimodal imaging of dynamic bone-tumor alterations associated with metastatic prostate cancer. PLoS One 2015; 10: e0123877.

[17] Galban CJ, Mukherji SK, Chenevert TL, Meyer CR, Hamstra DA, Bland PH, Johnson TD, Moffat BA, Rehemtulla A, Eisbruch A and Ross BD. A feasibility study of parametric response map analysis of diffusion-weighted magnetic resonance imaging scans of head and neck cancer patients for providing early detection of therapeutic efficacy. Transl Oncol 2009; 2: 184-190.

[18] Hamstra DA, Galban CJ, Meyer CR, Johnson TD, Sundgren PC, Tsien C, Lawrence TS, Junck L, Ross DJ, Rehemtulla A, Ross BD and Chenevert TL. Functional diffusion map as an early imaging biomarker for high-grade glioma: correlation with conventional radiologic response and overall survival. J Clin Oncol 2008; 26: 3387-3394.

[19] Moffat BA, Chenevert TL, Lawrence TS, Meyer CR, Johnson TD, Dong Q, Tsien C, Mukherji S, Quint DJ, Gebarski SS, Robertson PL, Junck LR, Rehemtulla A and Ross BD. Functional diffusion map: a noninvasive MRI biomarker for early stratification of clinical brain tumor response. Proc Natl Acad Sci U S A 2005; 102: 5524-5529.

[20] Lee KC, Bradley DA, Hussain M, Meyer CR, Chenevert TL, Jacobson JA, Johnson TD, Galban CJ, Rehemtulla A, Pienta KJ and Ross BD. A feasibility study evaluating the functional diffusion map as a predictive imaging biomarker for detection of treatment response in a patient with metastatic prostate cancer to the bone. Neoplasia 2007; 9: 1003-1011.

[21] Lee KC, Sud S, Meyer CR, Moffat BA, Chenevert TL, Rehemtulla A, Pienta KJ and Ross BD. An imaging biomarker of early treatment response in prostate cancer that has metastasized to the bone. Cancer Res 2007; 67: 3524-3528.

[22] Reischauer C, Froehlich JM, Koh DM, Graf N, Padevit C, John H, Binkert CA, Boesiger P and Gutzeit A. Bone metastases from prostate cancer: assessing treatment response by using diffusion-weighted imaging and functional diffusion maps--initial observations. Radiology 2010; 257: 523-531.

[23] Rozel S, Galban CJ, Nicolay K, Lee KC, Sud S, Neeley C, Snyder LA, Chenevert TL, Rehemtulla A, Ross BD and Pienta KJ. Synergy between anti-CCL2 and docetaxel as determined by DW-MRI in a metastatic bone cancer model. J Cell Biochem 2009; 107: 58-64.

[24] Eisenhauer EA, Therasse P, Bogaerts J, Schwartz LH, Sargent D, Ford R, Dancey J, Arbuck S, Gwyther S, Mooney M, Rubinstein L, Shankar L, Dodd L, Kaplan R, Lacombe D and Verweij J. New response evaluation criteria in solid tumours: revised RECIST guideline (version 1.1). Eur J Cancer 2009; 45: 228-247.

[25] Baschuk N, Rautela J and Parker BS. Bone specific immunity and its impact on metastasis. Bonekey Rep 2015; 4: 665.

[26] Graham TJ, Box G, Tunariu N, Crespo M, Spinks TJ, Miranda S, Attard G, de Bono J, Eccles SA, Davies FE and Robinson SP. Preclinical evaluation of imaging biomarkers for prostate cancer

bone metastasis and response to cabozan-tinib. J Natl Cancer Inst 2014; 106: dju033.

[27] Humphrey PA, Zhu X, Zarnegar R, Swanson PE, Ratliff TL, Vollmer RT and Day ML. Hepatocyte growth factor and its receptor (c-MET) in pros-tatic carcinoma. Am J Pathol 1995; 147: 386-396.

[28] Knudsen BS, Gmyrek GA, Inra J, Scherr DS, Vaughan ED, Nanus DM, Kattan MW, Gerald WL and Vande Woude GF. High expression of the Met receptor in prostate cancer metasta-sis to bone. Urology 2002; 60: 1113-1117.

[29] Qadan LR, Perez-Stable CM, Schwall RH, Burn-stein KL, Ostenson RC, Howard GA and Roos BA. Hepatocyte growth factor and vitamin D cooperatively inhibit androgen-unresponsive prostate cancer cell lines. Endocrinology 2000; 141: 2567-2573.

[30] Nishida N, Yano H, Nishida T, Kamura T and Kojiro M. Angiogenesis in cancer. Vasc Health Risk Manag 2006; 2: 213-219.

[31] Hoff BA, Bhojani MS, Rudge J, Chenevert TL, Meyer CR, Galban S, Johnson TD, Leopold JS, Rehemtulla A, Ross BD and Galban CJ. DCE and DW-MRI monitoring of vascular disruption following VEGF-Trap treatment of a rat glioma model. NMR Biomed 2012; 25: 935-942.

[32] Bauerle T, Bartling S, Berger M, Schmitt-Graff A, Hilbig H, Kauczor HU, Delorme S and Kiessling F. Imaging anti-angiogenic treatment response with DCE-VCT, DCE-MRI and DWI in an animal model of breast cancer bone metas-tasis. Eur J Radiol 2010; 73: 280-287.

[33] Maxwell RJ, Wilson J, Prise VE, Vojnovic B, Rus-tin GJ, Lodge MA and Tozer GM. Evaluation of the anti-vascular effects of combretastatin in rodent tumours by dynamic contrast en-hanced MRI. NMR Biomed 2002; 15: 89-98.

[34] Raatschen HJ, Simon GH, Fu Y, Sennino B, Shames DM, Wendland MF, McDonald DM and Brasch RC. Vascular permeability during anti-angiogenesis treatment: MR imaging assay results as biomarker for subsequent tumor growth in rats. Radiology 2008; 247: 391-399.

[35] Casanovas O, Hicklin DJ, Bergers G and Hana-han D. Drug resistance by evasion of antian-giogenic targeting of VEGF signaling in late-stage pancreatic islet tumors. Cancer Cell 2005; 8: 299-309.

[36] Hurwitz H, Fehrenbacher L, Novotny W, Cart-wright T, Hainsworth J, Heim W, Berlin J, Baron A, Griffing S, Holmgren E, Ferrara N, Fyfe G, Rogers B, Ross R and Kabbinavar F. Bevaci-zumab plus irinotecan, fluorouracil, and leu-covorin for metastatic colorectal cancer. N Engl J Med 2004; 350: 2335-2342.

[37] Ebos JM, Lee CR, Cruz-Munoz W, Bjarnason GA, Christensen JG and Kerbel RS. Accelerat-ed metastasis after short-term treatment with a potent inhibitor of tumor angiogenesis. Can-cer Cell 2009; 15: 232-239.

[38] Paez-Ribes M, Allen E, Hudock J, Takeda T, Okuyama H, Vinals F, Inoue M, Bergers G, Ha-nahan D and Casanovas O. Antiangiogenic therapy elicits malignant progression of tu-mors to increased local invasion and distant metastasis. Cancer Cell 2009; 15: 220-231.

[39] Shojaei F, Lee JH, Simmons BH, Wong A, Es-parza CO, Plumlee PA, Feng J, Stewart AE, Hu-Lowe DD and Christensen JG. HGF/c-Met acts as an alternative angiogenic pathway in suni-tinib-resistant tumors. Cancer Res 2010; 70: 10090-10100.

[40] Roodman GD and Silbermann R. Mechanisms of osteolytic and osteoblastic skeletal lesions. Bonekey Rep 2015; 4: 753.

[41] Guise TA. Molecular mechanisms of osteolytic bone metastases. Cancer 2000; 88: 2892-2898.

[42] Guise TA. The vicious cycle of bone metasta-ses. J Musculoskelet Neuronal Interact 2002; 2: 570-572.

[43] Zhao C, Irie N, Takada Y, Shimoda K, Miyamoto T, Nishiwaki T, Suda T and Matsuo K. Bidirec-tional ephrinB2-EphB4 signaling controls bone homeostasis. Cell Metab 2006; 4: 111-121.

[44] Tai S, Sun Y, Squires JM, Zhang H, Oh WK, Li-ang CZ and Huang J. PC3 is a cell line charac-teristic of prostatic small cell carcinoma. Pros-tate 2011; 71: 1668-1679.

[45] Even-Sapir E. Imaging of malignant bone in-volvement by morphologic, scintigraphic, and hybrid modalities. J Nucl Med 2005; 46: 1356-1367.